AO03: Looking for mountain-generated cloud

Chengyuan Zhang
Supervisors: Prof. D. Grainger

Abstract

This study investigates the evolution of orographic clouds over the Atlas Mountains, emphasizing the effective radius of water droplets within lee wave clouds. Employing the ESA Cloud Climate Change Initiative Retrieval Products, derived from Sentinel-3 satellite observations, this project uniquely focuses on the microphysical properties and dynamic behaviors of clouds affected by mountainous terrain. The research method integrates cloud effective radius and cloud top height measurements with advanced satellite instrumentation, allowing for precise characterization and analysis of cloud formations. Unexpected findings include a decrease in droplet size contrary to predictions based on the growth-by-condensation model, likely due to an increase in cloud top temperature facilitating droplet evaporation. This indicates complex interactions between cloud microphysics and atmospheric conditions that deviate from traditional models of orographic cloud formation. The results contribute to a better understanding of cloud dynamics in mountainous regions, which could significantly influence predictive models of weather and climate in such areas. Further studies could expand the scope of satellite data usage and incorporate diverse geographic locations to broaden our understanding of orographic cloud phenomena.

1 Introduction

When humid air is advected toward an orographic feature, such as a mountain, it undergoes forced ascent, resulting in adiabatic cooling. Should the moisture content of the air be adequate, saturation may be achieved, leading to the formation of a cap cloud at the mountain's summit. Subsequent to traversing the orographic barrier, the elevated air mass descends, during which process the cloud droplets undergo evaporation. This air mass then continues to experience vertical oscillations as it progresses downwind, giving rise to the formation of lee-wave clouds at the apex of each oscillation (figure 1). Contrary to the movement of the air mass, these clouds maintain a relatively stationary position [1].

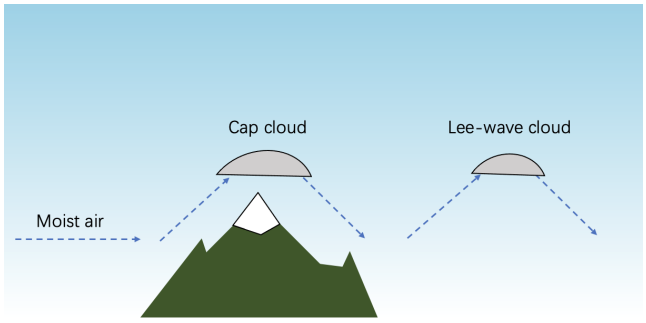

Figure 1: Clouds generated by mountains.

Orographic clouds may constitute the principal source of precipitation within mountainous regions. The maximal precipitation rates are usually observed on the windward side of the mountain, where forced ascent is the strongest. As the air mass descends, it undergoes warming and drying, thereby creating a rain shadow on the leeward side of the range [2].

Velocity and wave frequency are important properties of orographic clouds and have been intensively studied [3][4]. In contrast, the evolution of water particles in lee wave clouds has not received as much attention. This gap in the

literature underscores the need for our project, which aimed to examine orographic clouds generated at the Atlas Mountain. Specifically, we emphasized evaluating the effective radius of water droplets along the direction of lee wave cloud propagation.

For our analysis, we employed data from the ESA Cloud Climate Change Initiative (CCI) Retrieval Products. This level-2 product, derived from the Sea and Land Surface Temperature Radiometer (SLSTR) aboard the Sentinel-3 satellites, is integral to our research methodology. The advanced capabilities of this instrument allowed us to accurately measure and analyze cloud properties, providing valuable insights into the dynamics of cloud formation in this region.

2 Method

2.1 ESA Cloud CCI Retrieval Products

In this project, we leveraged the ESA Cloud CCI Retrieval Products, level-2 products processed through the Oxford-RAL Retrieval of Aerosol and Cloud (ORAC) system, which are instrumental to our analysis. The ORAC system utilizes a method that aligns a physically consistent cloud model with satellite observations across the spectrum, from the visible to the mid-infrared [5]. This approach ensures the accurate representation of cloud dynamics as observed by the Sentinel-3 satellites' Sea and Land Surface Temperature Radiometer (SLSTR). Specifically, the critical parameter of cloud effective radius was derived using an Optimal Estimation Method (OEM), applied to the visible channels of the SLSTR, facilitating precise measurement of this key cloud characteristic.

Additionally, cloud top height, another vital metric for our study, is determined from stereoscopic observations made possible by the SLSTR's multiple viewing angles. This capability underscores the Sentinel-3 satellites' advanced observational technologies, enhancing our understanding of cloud structures and behaviors.

The Sentinel-3 satellites operate in a near-polar, sun-synchronous orbit, with a descending node equatorial crossing at 10:00 h Mean Local Solar Time, at an orbit inclination of 98.65°. This strategic orbiting pattern ensures consistent, global coverage and observation conditions, contributing to the comprehensive dataset each retrieval file presents. With each file containing 1,800,000 pixels at a 1 km resolution, our dataset offers unparalleled granularity and scope for analyzing cloud properties, enabling detailed insights into cloud formation and dynamics over the Atlas Mountain region.

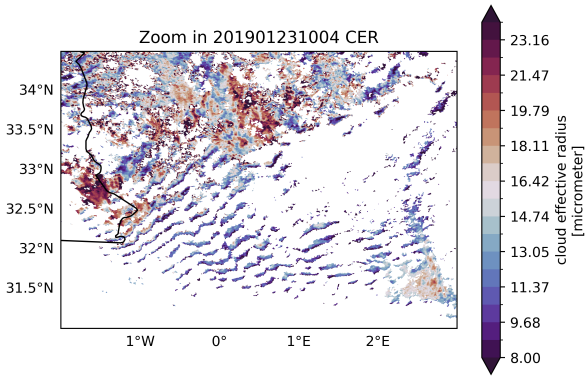

Figure 2: Contour map of clouds effective radius in North Africa shows the lee-wave cloud above Atlas mountain. (2019.01.23)

2.2 Growth by Condensation

A good approximation describe the growth of water particle by condensation is

$$r\frac{dr}{dt} = \frac{(S - 1 - \frac{a}{r} + \frac{b}{r^3})}{[F_k + F_d]} \tag{1}$$

where $S = e/e_s(T)$ is the ambient saturation ratio; a/r and b/r^3 are terms associated with the solution and curvature effects on the particle's equilibrium vapor pressure; F_k and F_d

are associated with heat conduction and vapor diffusion [6].

For a sufficiently large droplet, the a/r and b/r^3 terms are negligible compared to $(S-1)$ so we have

$$r\frac{dr}{dt} = \frac{S-1}{[F_k + F_d]} \tag{2}$$

which can be integrate to give

$$r(t) = \sqrt{r_0^2 + 2\xi t} \tag{3}$$

where

$$\xi = \frac{S-1}{[F_k + F_d]}. \tag{4}$$

The horizontal wind velocity varying slowly [7] so we can write the relationship between droplet radius and the distance from cloud edge

$$r(d) = \sqrt{r_0^2 + 2\xi \frac{d}{v_h}} \tag{5}$$

where v_h is the horizontal wind velocity in lee wave clouds.

3 Results

3.1 Sampling Strategy

The structure of real lee wave clouds is markedly influenced by the topography of the mountain where the orographic cloud formation begins (figure 2), as opposed to idealized lee wave clouds which are parallel. Recognizing this, our study focuses on the evolution of cloud effective radius within lee wave clouds, specifically targeting areas where clouds demonstrate relatively homogeneous characteristics (figure 3). This decision was made to ensure that our analysis could more accurately reflect the influence of lee waves on cloud properties without the added complexity of variable cloud structures.

To facilitate this, we employed a systematic sampling approach across the selected cloud formations. Our methodology included the establishment of 50 parallel vectors, with 800

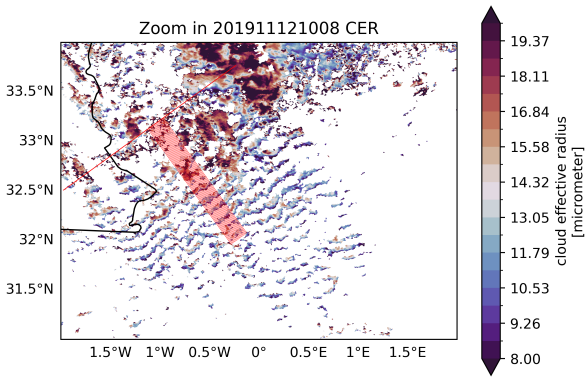

Figure 3: Sampling area. (2019.11.12)

sampling points distributed along each vector. The sampling algorithm was designed to identify the retrieval file's pixel closest to each sampling point. The deviation in longitude (λ) and latitude (ϕ)

$$\delta = |\lambda_d - \lambda_s| + |\phi_d - \phi_s| \tag{6}$$

is minimised. Subsequently, the data collected along each vector are grouped by distance from the starting point and averaged, resulting in plots of variables against distance from the initial point. This precision in sampling is crucial for accurately tracking the changes in cloud effective radius as the lee wave propagates.

The masks used for selecting valid data are shown in table 1.

Phase	Water
Quality	Retrieval converge Particle type consist
Validity*	>80%
CER Uncertainty	<40

* : The percentage of valid data at certain distance.

Table 1: Data masks.

3.2 Cloud Effective Radius

The averaged cloud effective radius along each sampling vector, as illustrated in figure 3, is

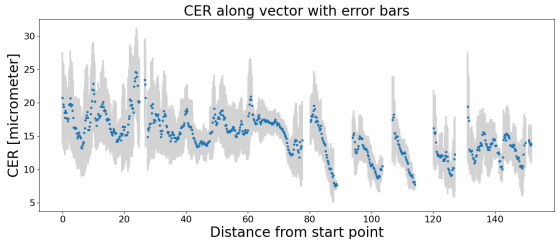

(a) Averaged cloud effective radius along sampling vector in figure 3.

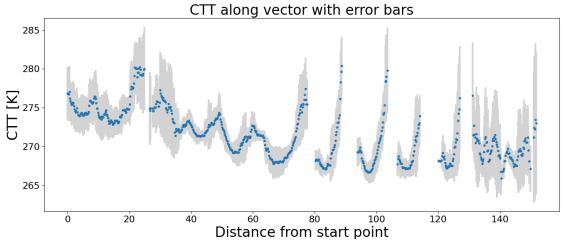

(b) Averaged cloud top temperature along sampling vector in figure 3.

Figure 4: Cloud effective radius and cloud top temperature along sampling vector in figure 3.

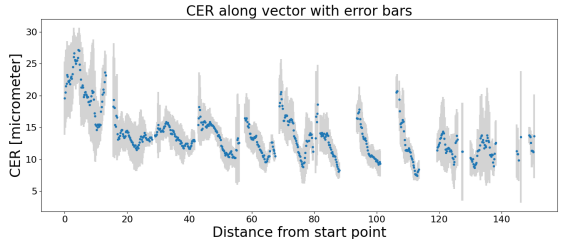

(a) Averaged cloud effective radius along sampling vector in figure 5.

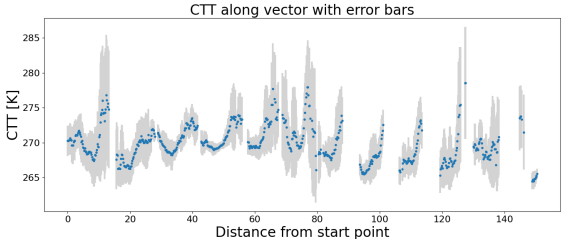

(b) Averaged cloud top temperature along sampling vector in figure 5

Figure 6: Cloud effective radius and cloud top temperature along sampling vector in figure 5

further detailed in figure 4a. Contrary to our expectations based on Equation 5, the observed trends diverge significantly from the anticipated patterns. This deviation becomes even more pronounced when examining an additional sampling group, as depicted in figures 5 and 6a. Instead of observing an increase in droplet radius from the cloud edge, as initially hypothesized, there is a notable decrease in droplet size.

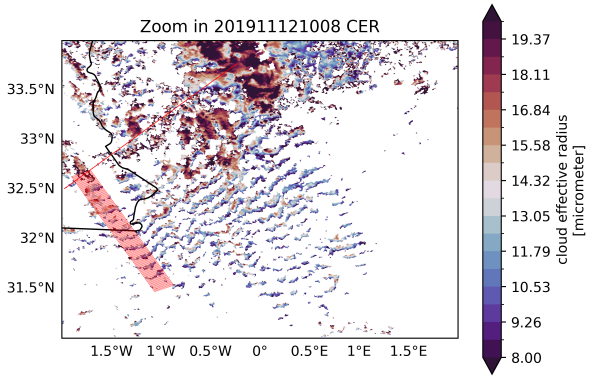

Figure 5: Another sampling area. (2019.11.12)

The unexpected decrease in droplet size, initially observed in figures 4a and 6a, can be rationalized by examining the cloud top temperature. As illustrated in figures 4b and 6b, there is an increase in cloud top temperature when moving away from the cloud edge. This rise in temperature leads to an increase in saturation vapor pressure, creating conditions conducive to the evaporation of larger droplets, which subsequently become smaller. This process explains the reduction in droplet size despite initial expectations of an increase.

3.3 Temperature Profile

Figure 8 presents the temperature profile derived from the cloud top temperature and cloud top height. The relationship between temperature (T) and altitude (H) is modeled through linear regression, resulting in the following equation:

$$T = -5.32H + 290.4. \tag{7}$$

The intercept at 290.4 °K corresponds accurately with the observed surface temperature.

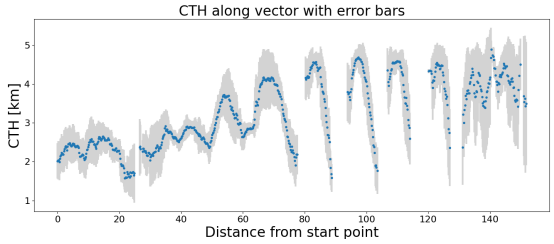

(a) Averaged cloud top height along sampling vector in figure 3.

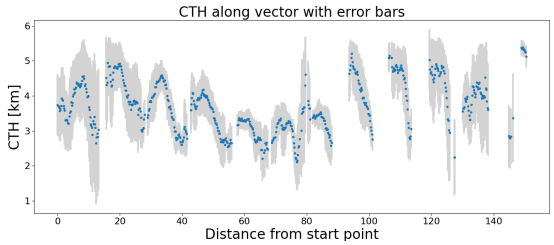

(b) Averaged cloud top height along sampling vector in figure 5

Figure 7: Cloud top height along sampling vector in figure 3 and figure 5

Furthermore, the slope of -5.32 °K/km is consistent with a typical moist adiabatic lapse rate, as discussed in existing literature [8].

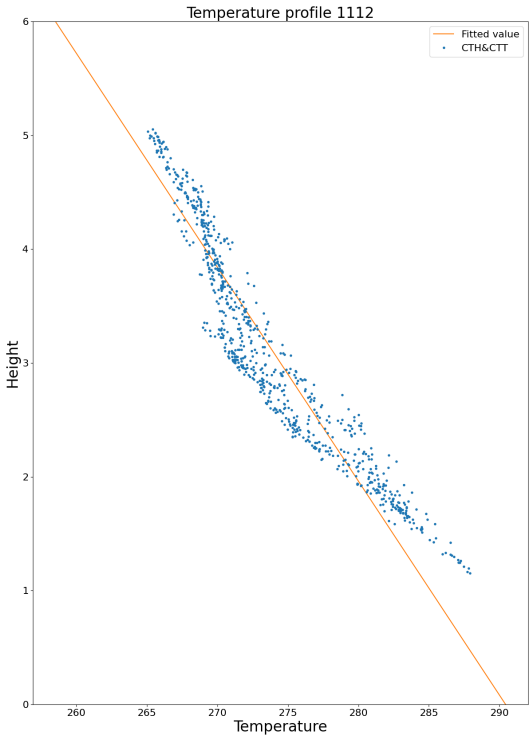

Figure 8: Cloud top temperature and cloud top height data and fitted temperature profile.

3.4 Uncertainty

The retrieval method introduces edge effects, which significantly increase the uncertainty of the results, potentially exceeding 100% [5]. figure 9 illustrates the uncertainty in the retrieved results of the cloud effective radius after data screening. It can be observed that the level of uncertainty is relatively low in two specific sampling areas.

Given that the analysis averages data from 50 vectors, it is crucial to recognize that data at a specific distance may not always originate from the same cloud. This is particularly evident when the cloud's parallel structure is obscure at the front and back ends of the sampling vectors. Figures 4a and 6a illustrate that the standard deviation is notably lower in regions where the clouds exhibit relatively homogeneous characteristics.

3.5 Discussion

3.5.1 Unstable Air Aloft

The characteristics of the cloud top height, as depicted in figures 7a and 7b, suggest that these formations are cumulus clouds. This observation can be attributed to strong thermal lifting, where a moist air mass ascends rapidly [9]. This rapid upward movement is a plausible explanation for the observed cap cloud shape on the windward side of the mountain.

However, the formation of such orographic clouds typically does not lead to the development of lee wave clouds downstream. The presence of cumulus clouds, indicative of unstable air conditions aloft, raises questions about the typical formation processes of lee wave clouds, suggesting that different mechanisms may be at play in these observed instances.

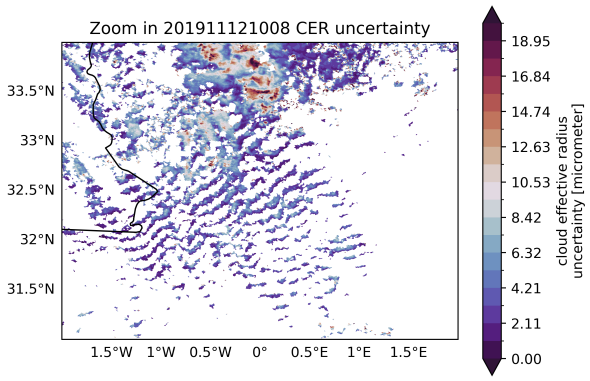

Figure 9: Cloud effective radius uncertainty.

3.5.2 Wave Clouds at Different Levels

The orographic impact on airflow can extend significantly beyond the peak or crest levels of mountains, potentially generating one or several lenticular, orographically-shaped clouds at altitudes much higher than the mountain itself. These formations, known as lenticular clouds, are indicative of wave clouds that form at different levels due to the orographic disturbance of stable airflows. Such structures, however, might not always be captured or clearly reflected in the retrieval data due to their elevated positions and the specific parameters being measured.

However, the measurements of cloud top height available from our data do not indicate any anomalous elevations that would suggest the presence of such elevated lenticular clouds.

4 Conclusion

This project aims to enhance our understanding of orographic cloud evolution by analyzing the effective radius along the direction of lee wave cloud propagation. Contrary to the initial assumption of growth via condensation, an anomalously rapid increase in the effective radius was observed at the onset of orographic cloud formation, followed by a gradual evaporation. Further investigation of cloud top height and cloud top temperature revealed that the clouds assume an unexpected shape. In response, I propose two hypotheses, though neither fully accounts for the observed phenomena.

Future research could expand on this study by incorporating more case studies of orographic clouds, given that the SLSTR data from 2019 contains limited instances over the Atlas Mountains. It would be beneficial to cross-reference this data with other sources, such as MODIS. Additionally, studying orographic clouds in various global locations may help elucidate the influence of climate on their characteristics.

References

[1] Roland Stull (2017). *Practical Meteorology: An Algebra-based Survey of Atmospheric Science*. University of British Columbia. ISBN 978-0-88865-283-6.

[2] C. David Whiteman (2000). *Mountain Meteorology: Fundamentals and Applications*. Oxford University Press. ISBN 0-19-513271-8.

[3] Larsén, X., Larsen, S., and Hahmann, N. A.: Origin of the waves in "A case study of mesoscale spectra of wind and temperature, observed and simulated": lee waves of the Norwegian mountains, Q. J. Roy. Meteor. Soc., 138, 274–279, https://doi.org/10.1002/qj.916, 2012a.

[4] C. Guo, W. Ai, S. Hu, X. Du and N. Chen, "Sea surface wind direction retrieval based on convolutional neural network and wavelet analysis", IEEE J. Sel. Topics Appl. Earth Observ. Remote Sens., vol. 15, pp. 3868-3876, 2022.

[5] Poulsen, C. A., Siddans, R., Thomas, G. E., Sayer, A. M., Grainger, R. G., Campmany, E., Dean, S. M., Arnold, C., and Watts, P. D.: Cloud retrievals from satellite data using optimal estimation: evaluation and application to ATSR, Atmos. Meas. Tech., 5,

1889–1910, https://doi.org/10.5194/amt-5-1889-2012, 2012.a, b

[6] R. R. Rogers, M. K. Yau, A Short Course in Cloud Physics (pp. 101-104), International series in natural philosophy. ISBN 0-08-034863-7.

[7] Millane, R. P. , Stirling, G. D. , Brown, R. G. , Zhang, N., Lo, V. L. , Enevoldson, E., and Murray, J. E. , 2010, "Estimating Wind Velocities in Mountain Lee Waves Using Sailplane Flight Data," J. Atmos. Oceanic Technol., 27, pp. 147–158.

[8] Minder, JR; Mote, PW; Lundquist, JD (2010). "Surface temperature lapse rates over complex terrain: Lessons from the Cascade Mountains". J. Geophys. Res. 115 (D14): D14122. Bibcode:2010JGRD..11514122M. doi:10.1029/2009JD013493

[9] World Meteorological Organization. "Orographic Influences on the Windward Side." Cloud Atlas, [17 Apr. 2024]. https://cloudatlas.wmo.int/en/orographic-influences-on-the-windward-side.html.